Experimental Validation of Unsteady Pressure-Sensitive Paint for Acoustic Applications

Jan Gößling[a], Thomas Ahlefeldt[b], Michael Hilfer[b]

[a]*Leibniz University Hannover, Institute of Turbomachinery and Fluid Dynamics, Hannover, Germany*
[b]*German Aerospace Center (DLR), Institute of Aerodynamics and Flow Technology, Göttingen, Germany*

Abstract

Fast response Pressure-Sensitive Paint (iPSP) developed at the German Aerospace Center (DLR) in Göttingen is evaluated for measurements of acoustic pressure distributions. A test facility is constructed, which allows to measure these acoustic pressure distributions with iPSP. The aim of this evaluation is to detect pressure amplitudes below 100 Pa with sinusoidal and white noise acoustic excitation between 1 and 4 kHz. The following data analysis methods are applied to increase the signal-to-noise ratio (SNR): phase averaging, proper orthogonal decomposition (POD), dynamic mode decomposition (DMD), and fast Fourier transform (FFT). DMD is identified to be very powerful in extracting acoustic pressure fluctuations and eliminating image noise, but FFT achieves comparable results in this application. The used measurement setup combined with the DMD or FFT are capable of detecting pressure levels below 11 Pa or 114 dB sound pressure level (SPL) in cases with white noise excitation with detected mode frequencies up to 4615 Hz. The minimal detectable pressure limit during this investigation is 5 Pa or 108 dB (SPL) at 1318 Hz and sinusoidal acoustic excitation. The results from iPSP are compared to conventional measurement technique, flush with the surface mounted microphones, with good agreement.

Keywords:
Pressure Sensitive Paint, acoustic, surface measurement, data analysis, Proper Orthogonal Decomposition, Dynamic Mode Decomposition, DMD, POD, FFT, iPSP, SPL

PSP	Pressure-Sensitive Paint
iPSP	fast response Pressure-Sensitive Paint
DLR	German Aerospace Center
AWT	Aeroacoustic Wind Tunnel
UV	ultraviolet
LED	light-emitting diode
PC	polymer/ceramic
SPL	sound pressure level
SNR	signal-to-noise ratio
STD	standard deviation
PMT	photomultiplier tube
FFT	fast Fourier transform
CCD	charge-coupled device
CMOS	complementary metal-oxide-semiconductor
SVD	singular value decomposition
POD	proper orthogonal decomposition
DMD	dynamic mode decomposition
COP	coherent output power
DFT	discrete Fourier transform
PSD	power spectral density
DTFT	discrete-time Fourier transform

1. Introduction

In the research of aerodynamics the experimental investigation of surface pressures is indispensable for the understanding of principal flow phenomena. Also in acoustic applications the study of surface pressure distribution is mandatory to understand noise sources, noise propagation and other phenomena. Typically, pressure is measured at discrete positions with e.g. pressure taps situated on the investigated surface. To accomplish an acceptable pressure information on complex geometries hundreds of sensors are needed.
Pressure-Sensitive Paint (PSP) is an established measurement technique to investigate pressure distribution on a surface with a high spatial resolution. Acoustic measurements using PSP are particularly challenging since PSP is an absolute pressure sensor and the acoustic pressure fluctuations are low compared to the ambient pressure. In this work an investigation of fast response Pressure-Sensitive Paint (iPSP) developed at German Aerospace Center (DLR) in Göttingen is performed to measure

Email address: michael.hilfer@dlr.de (Michael Hilfer)

acoustic pressure fluctuations similar to those found inside the Aeroacoustic Wind Tunnel (AWT), Leibniz University Hannover. To simulate those conditions inside the test setup, two speakers are used to induce pressure fluctuations between 1000 and 5000 Hz with pressure levels up to 400 Pa or 146 dB (SPL).

1.1. Basic Principles of Pressure-Sensitive Paint

PSP is an optical pressure measurement technique based on a photo-physical phenomenon of luminophores. Exciting the paint by light with a certain wavelength, the luminiphores in the paint emit light with longer wavelength, Liu and Sullivan (2005). Another method of how the excited luminophore can lose its absorbed energy is oxygen quenching. Oxygen quenching is a process in which the energy from the excited luminophore is transferred to a nearby oxygen molecule without emitting a photon in visible range, Gregory et al. (2014). With higher oxygen concentration around the surface, the oxygen quenching is more likely to happen and less light is emitted by the luminophores. According to Henry's law, the concentration of oxygen in the paint layer is proportional to the pressure on the surface. By having a constant oxygen concentration in the gas above the surface, the pressure is directly related to the luminescence intensity of the PSP luminophores.

1.2. Intensity Method

There are two methods to measure pressure distribution with PSP; intensity and lifetime method. The intensity method is used in this work and requires a continuous illumination of the paint. The intensity of the light emission is measured by a camera. To determine the pressure from the registered images, the Stern-Volmer equation

$$\frac{I_{ref}}{I} = A + B\frac{p}{p_{ref}} \tag{1}$$

is used with predetermined temperature dependent coefficients A and B.

1.3. Fast Response Pressure-Sensitive Paint and Low Pressure Applications

Acoustic measurements with iPSP are especially challenging because of the high frequencies and the low pressure fluctuations compared to the high ambient pressure. Previous measurements conducted inside the AWT reached sound pressure levels (SPLs) of up to 136 dB (126 Pa), Bartelt et al. (2013). With an ambient pressure of 10^5 Pa the absolute pressure change is only 0.126%. Therefore, absolute pressure sensors with a high SNR are required.

McGraw et al. (2003) were measuring acoustic resonance inside a cylinder with iPSP. The pressure field was induced by a speaker with frequencies between 150 and 3500 Hz. The iPSP was continuously excited by an ultraviolet (UV)-light-emitting diode (LED) and the changing intensity of emitted light was captured by a photomultiplier tube (PMT). The data of the point measurement was averaged and analysed via the FFT. The results were compared to a reference microphone. McGraw et al. (2003) were able to measure acoustic pressure fluctuations above 110 dB (6.32 Pa) with frequencies up to 3500 Hz.

To utilize the high spatial resolution advantage of PSP over conventional microphones, the PMT has to be replaced with a high speed camera. Gregory et al. (2006) were using a 14-bit charge-coupled device (CCD) camera to record the intensity changes of a standing wave in a rectangular cavity induced by a compression driver. The 100 W compression driver induced the mode (1 1 0) with a frequency of 1.3 kHz. Mode (1 1 0) appears when exactly half of the wavelength of the sound waves fits between the walls in x and y direction. In this test fast response polymer/ceramic (PC)-PSP was coated on the back wall of the cavity and excited by a pulsed UV-LED. A total of 200 images were phase averaged and a 10 pixel square area was average to increase the signal-to-noise ratio (SNR). The resulting iPSP data was compared to an analytic solution and a measurement of one fast response pressure sensor (Kulite) situated in a corner of the cavity. The minimum detectable pressure in this test was 115.8 dB (12.3 Pa).

To further enhance the SNR of iPSP data and investigate lower pressure magnitudes Pastuhoff et al. (2013) were using singular value decomposition (SVD).

SVD is part of linear algebra and separates the matrix A into three matrices U, Σ and W (Strang, 2003). A can be recalculated with the equation

$$A = U\Sigma W^T = \sum_{i=1}^{N} \sigma_i u_i w_i^T, \tag{2}$$

where U and W contain the left and right singular vectors u_i and w_i and diagonal entries of Σ contains the square root of the eigenvalues σ_i sorted with descending magnitude. By recalculating the matrix A using only modes with a high magnitude, the SNR can be improved, since the noise is contained in eigenvalues with low magnitudes. Pastuhoff et al. (2013) investigated the fluctuating pressure field on the side of a square cylinder at low speed flow and improved the SNR by using SVD.

In order to investigate multi frequency phenomena, different data analysis methods need to be applied. Peng et al. (2016) presented a measurement of wall-pressure fluctuations in low-speed flows as low as 10 m/s. They successfully employed and compared FFT, phase-averaging and POD, a related method to SVD, on structures measured by iPSP and caused by the wake of a cylinder. A POD mode is a left singular vector of the SVD and can be calculated with the known SVD algorithm. They compared POD filtered and reconstructed data to microphone measurements with good agreement. Ali et al. (2016) used POD and DMD to reduce the noise and measure multi frequency phenomena. DMD calculation using flow field data is well described by Schmid (2010) and can be used in similar procedure for pressure field data.

The experimental setup used by Ali et al. (2016) is similar to the setup of Gregory et al. (2006), which includes an excitation of standing waves (modes) inside a rectangular cavity, except a second speaker is mounted at the side of the box for resonance with two different frequencies. The principles of

POD and DMD are described and their results compared to each other, the phase averaging method, and the analytic solution. It is notable that both methods were able to separate two different modes induced simultaneously. According to Ali et al. (2016), DMD is the more robust method in discriminating between the two modes and eliminating the noise of the CMOS sensor.
Noda et al. (2018) measured trailing edge noise of a NACA0012 wing profile with iPSP and analysed the data with the coherent output power (COP) method. COP uses the iPSP data and the amplitude and phase information of a separate microphone located behind the wing. Therefore, the SNR was significantly higher than using the averaging method. Noda et al. (2018) were capable of detecting power spectra amplitudes of 20 Pa^2. Disotell and Gregory (2011) presented a measurement of two dimensional unsteady pressure distribution inside the same cavity as Gregory et al. (2006), using a single-shot lifetime technique. They were able to detect transient pressure fluctuations exited by a 1.3 kHz acoustic excitation for different phase angles with pressure amplitudes above 154 dB SPL (1000 Pa). Using phase averaging the used setup was able to resolve pressure amplitudes of 125.4 dB SPL (52.7 Pa).

2. Experiment

2.1. Test facility

The measurement of acoustic pressure distributions inside the AWT requires a setup which can detect pressure levels up to 126 Pa (136 dB) and multiple frequencies between 1000 Hz and 4000 Hz. To investigate the iPSP in similar conditions, a new test facility is built. Ali et al. (2016) already measured acoustic pressure distributions with multiple frequencies inside a rectangular cavity. They induced pressure amplitudes above 600 Pa with frequencies up to 2200 Hz. The dimensions of the test section are 216 mm in width, 168 mm in height and 102 mm in depth. In order to predict if such rectangular cavity is capable of providing the right measurement conditions, an analytic solution of the acoustic phenomena inside the cavity is calculated. The theoretical excitation frequency of a mode inside a rectangular cavity is given by the solution of the Helmholz equation (Pierce, 1981) with,

$$f = \frac{c}{2}\sqrt{\left(\frac{n_x}{L_x}\right)^2 + \left(\frac{n_y}{L_y}\right)^2 + \left(\frac{n_z}{L_z}\right)^2} \tag{3}$$

where L_x, L_y, and L_z are the length, height, and depth in the x, y, and z direction, respectively; n_x, n_y, and n_z representing the mode number along their dimensions; and c is the speed of sound. By using the same dimensions for the test section as Ali et al. (2016), 70 modes with frequencies ranging from 1029 Hz to 4910 Hz can be excited. 28 of these modes induce distinct pressure distributions on the back wall. The modes are well distributed with single modes in a 300 Hz frequency band and with some close modes, e.g. mode (2 2 0) and (3 1 0) with frequencies of 2607 Hz and 2614 Hz, respectively. Investigations of the modes (1 1 0), (1 2 0), and (2 1 0) have already been published by Ali et al. (2016) and can be used for comparison. Therefore, the setup to reproduce AWT similar acoustic conditions is a rectangular cavity, further designated as acoustic box, with the same dimensions as in the tests of Gregory et al. (2006), Disotell and Gregory (2011), and Ali et al. (2016).

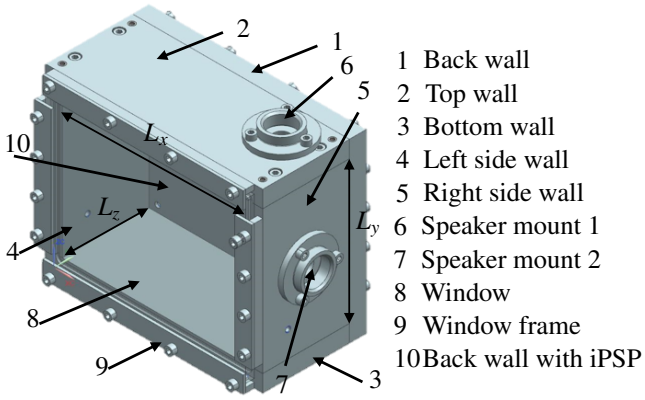

Figure 1: 3D CAD construction of the acoustic box

The 3D CAD construction of the test facility is shown in Fig. 1.
The pressure distribution on the back wall of the acoustic box is investigated with iPSP. For later comparison and verification of the pressure on the back wall, a second pressure measurement technique is included. To measure acoustic phenomena precisely Möser (2012) suggest condenser microphones. The microphones are mounted in different positions on the back wall of the box. The number of microphones and their position can be determined with the analytic solution of the pressure distribution inside the acoustic box. The theoretical pressure distribution of a specific mode can be calculated with the equation

$$P(x, y, z) = cos\left(\frac{n_x \pi x}{L_x}\right) cos\left(\frac{n_y \pi y}{L_y}\right) cos\left(\frac{n_z \pi z}{L_z}\right) \tag{4}$$

shown by Pierce (1981). The microphone positions are obtained by calculating the pressure distributions of the modes inside the frequency band given by the AWT with Eq. 4. The resulting absolute values of the modes, with a maximum mode number of three, are added.

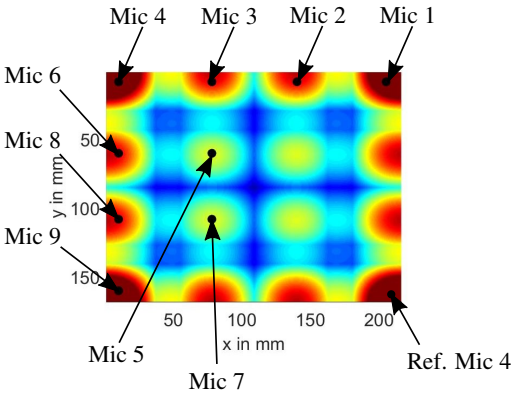

Figure 2: Overlapped modes to determine microphone positions

This leads to a point symmetric pressure distribution shown in Fig. 2. Nine microphones, represented by the black dots,

are placed in the resulting convexities. The Nyquist-Shannon sampling theorem for modes with a mode number of four and lower is satisfied with the chosen microphone positioning. Due to the symmetry of the modes, every microphone has a reference position on the back wall to compare with. The signal of the microphones and the signal of the iPSP at the reference position can be correlated to each other and a pressure recalculation of the iPSP with the microphones is possible.
The oxygen level of the air inside the acoustic box has also an effect on the calibration and sensitivity of the iPSP. By flushing the box with synthetic air with a known oxygen level of 20%, an oxygen meter is not required. This also ensures dry air conditions inside the box, which is part of the assumption for the analytic calculations of modes, Pierce (1981). One temperature sensor (Pt100) and one absolute pressure sensor are added to the test facility to ensure that the facility is always operated at the same temperature and pressure conditions. Same temperature is ensured by waiting after each flushing until the equilibrium with the temperature inside the laboratory is reached. This way, the influence of temperature on the iPSP response characteristic is minimised. Since during the operation the LEDs are only switched on for the duration of the image acquisition ($t_{ON} < 1s$), no detectable temperature changes inside the box are observed.

2.2. *Instrumentation*

The paint developed by the DLR is coated on the back wall of the acoustic box. The recipe is a modification of the paint developed by Gregory (2004). It consist of a polymer/ceramic base layer and an active layer. The base layer is a mixture of a polymer (Duromax B-1000), a ceramic particle (titanium silicon oxide $TiSiO_4$, 50 nm), dispersant (Aldrich PANa 4160029) and distilled water. The active layer includes toluene and the luminophore PtTFPP. Base layer and active layer are subsequently coated on the surface of the back wall creating a coating as shown in Fig 3.

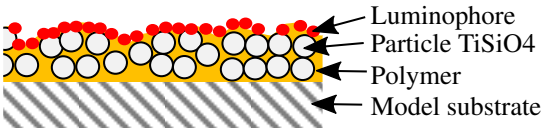

Figure 3: Sketch of iPSP paint composition

The luminophore is excited by a LED light source with a central wavelength of 390 nm and features an emission peak at the wavelength of 650 nm.
The devices required for the iPSP measurement are one high speed complementary metal-oxide-semiconductor (CMOS) camera and two UV-LEDs equipped with lenses and optical filters.

The two UV-LEDs are HardSoft IL-106 UV, emitting light at a wavelength of 390 nm. The LEDs are equipped with 720 mm lenses and optical band-pass filters. The filters are selected to pass light with wavelength between 380 nm and 400 nm and are

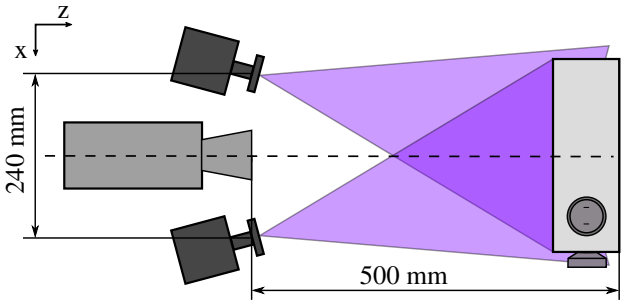

Figure 4: Installation of the LEDs and the camera

mounted on the front of the lenses. The LEDs are placed beside the camera and angled towards the acoustic box as shown in Fig. 4, so that the whole back wall is illuminated. The angle between the z axis and the LED is 13.8°. The distance between the LEDs and the acoustic box is 500 mm. The LEDs are 240 mm apart in x direction.
The camera is a Photron Fastcam SA-Z, equipped with a Nikon 85 mm lens and a band-pass filter passing light with wavelength from 640 nm to 660 nm. The camera is set to record 9000 images with a resolution of 768 x 768 pixel. The maximum frame rate at this resolution is 32 kHz. The used image sensor is a CMOS sensor with 12 bit dynamic range. The camera can be triggered and synchronised.
To obtain pressure references and calibration information for the iPSP measurement, nine calibrated microphones, an absolute pressure sensor, and a temperature sensor are used. The used microphones are Brüel&Kjaer Type 4944 1/4" microphones with a dynamic range of 46 dB to 170 dB and detectable frequencies between 4 Hz and 70,000 Hz. The microphones are distributed as shown in Fig. 2 and mounted without the protection grid flush to the surface. The microphone signals are simultaneously sampled by the VIPER HD data acquisition system with an A/D conversion of 24 bits and a sampling frequency of 240 kHz. The recording period for the investigated measurement is 20 seconds.
The modes inside the acoustic box are excited with two BMS 4540ND - 8Ω speakers. The placement of the speakers has only a small influence on the modes inside the rectangular cavity (Ali et al., 2016), so the speakers are arranged similar to the measurement of Ali et al. (2016). The top speaker is located at $\frac{x}{L_x} = 0.9$, $\frac{y}{L_y} = 1$, and $\frac{z}{L_z} = 0.5$ and the side speaker at $\frac{x}{L_x} = 1$, $\frac{y}{L_y} = 0.5$, and $\frac{z}{L_z} = 0.5$. Each speaker can induce frequencies from 700 Hz to 30 kHz. The maximum achievable continuous free field SPL is 132 dB with a power of 60 W. The speakers are driven by a signal generated by the function generator Agilent 33522A. The signal from the generator is filtered and amplified.
All voltage signals are logged with a data logging system. The data logger is the Viper HDR, which can sample with a maximal sampling rate of 250 kHz. It has 64 analogue input channels with a resolution of 24 bit and is logging the signals of the nine microphones, the absolute pressure sensor, the signal of the function generator, and signals from the camera. The signals from the camera are Synch Out Pos, Expose Pos and Trig Pos, which are a synchronisation signal, the camera's exposure sig-

nal, and the output of the received trigger signal, respectively.

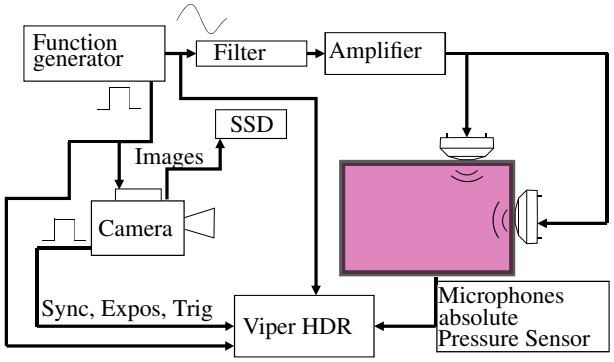

Figure 5: Synchronisation diagram of the measurements

Since the camera is recording with frequencies up to 32 kHz, high sampling rates for the camera output signals are required. The synchronisation of the measurement is shown in Fig. 5 and consist of the function generator, generating two in phase signals. One sinusoidal signal is driving the speakers and the second signal is a square wave, which is synchronising the camera with the speakers. This is only done, when a specific mode is excited and not during the white noise measurement. When the speakers are driven with a white noise signal, the camera is running independently. In both cases the output signals are logged and a post processing synchronisation can be carried out.

3. Data Analysis Methods

3.1. Microphone Data - Power Spectral Density

To obtain the SPL of a specific mode the power spectral density (PSD) is calculated. The PSD is used to estimate the total power distribution from a finite sample of stationary phenomena. Stoica and Moses (2005) define the PSD as the discrete-time Fourier transform (DTFT) of the covariance sequence with,

$$\phi(\omega) = \sum_{k=-\infty}^{\infty} x(k) e^{-i\omega k} \tag{5}$$

including a discrete set of real or complex numbers $x(k)$, for all integers k, and the angular frequency ω.
The PSD is calculated with the Welch's power spectral density estimation. The method includes sectioning, taking modified periodograms of these sections and averaging these modified periodograms (Welch, 1967).

3.2. Singular Value Decomposition and Proper Orthogonal Decomposition

The singular value decomposition and its value for increasing the SNR during iPSP measurements is described in Sec. 1.3. The mathematical principle is further described by Strang (2003). Equation 2 can be calculated numerically with MATLAB by using the inbuilt *svd* function. The resulting matrices U, S, and W contain the left singular vectors, the singular values, and the right singular vectors, respectively. The singular values are sorted by their energy in a descending order and are the square roots of the eigenvalues. The left singular values are also known as the proper orthogonal decomposition (POD) modes. The POD mode u_i describes the pressure fluctuation of the singular value s_i. They contain several frequencies. The included frequencies can be obtained by calculating the single sided frequency spectrum of the right singular vector w_i.

3.3. Dynamic Mode Decomposition (DMD)

The dynamic mode decomposition is introduced in Sec. 1.3. To calculate the DMD the data is given by a matrix V_1^N,

$$V_1^N = v_1, v_2, v_3, ..., v_N, \tag{6}$$

in form of a snapshot sequence, where v_i stands for the *ith* pressure field. The time Δt between each snapshot is constant. The decomposition is based on a linear assumption that a pressure field v_i is mapped with a matrix A to a subsequent pressure field v_{i+1}, that is,

$$v_{i+1} = A v_i \tag{7}$$

and A is constant for the whole interval. Due to the constant mapping the snapshot sequence can also be expressed as a Krylov sequence,

$$V_1^N = \{v_1, Av_1, A^2 v_1, ..., A^{N-1} v_1\}. \tag{8}$$

The dynamic characteristic of the pressure field can be investigated by calculating the eigenvalues and eigenvectors of A. By increasing the number of snapshots, the linear dependency is approached for the data set and the last vector v_N can be expressed by

$$v_N = a_1 v_1 + a_2 v_2 + ... + a_{N-1} v_{N-1} + r \tag{9}$$

as a linear combination of the previous and linear independent vectors v_i, with $i = 1, ..., N-1$. Equation 9 can also be written in matrix form that is,

$$v_N = V_1^{N-1} a + r \tag{10}$$

with $a^T = \{a_1, a_2, ..., a_{N-1}\}$ and r as the residual vector. By following Ruhe (1984) the equation 10 can be written in

$$\begin{aligned} A\{v_1, v_2, v_3, ..., v_{N-1}\} &= \{v_2, v_3, v_4, ..., v_N\} \\ &= \{v_2, v_3, v_4, ..., V_1^{N-1} a\} + r e_{N-1}^t \end{aligned} \tag{11}$$

or in matrix form

$$A V_1^{N-1} = V_2^N = V_1^{N-1} S + r e_{N-1}^T \tag{12}$$

with $e_{N-1} \in \mathbb{R}^{N-1}$ as the $(N-1)$th unit vector. The matrix S in Equation 12 is a low dimensional representation of the matrix A and shifts the snapshot sequence index from one to $N-1$.

$$S = \begin{pmatrix} 0 & & & & a_1 \\ 1 & 0 & & & a_2 \\ & \ddots & \ddots & & \vdots \\ & & 1 & 0 & a_{N-2} \\ & & & 1 & a_{N-1} \end{pmatrix}. \tag{13}$$

The eigenvalues λ_i of S approximate some of the eigenvalues of the full system matrix A (Schmid, 2010). A robust method is to calculate a matrix $\tilde{S}$, which is related to S, by using the SVD of the snapshot sequence V_1^{N-1} with

$$V_1^{N-1} = U\Sigma W^T. \tag{14}$$

By neglecting the residual term re_{N-1}^T and substituting equation 14 into equation 11, the equation

$$V_2^N = U\Sigma W^T S \tag{15}$$

is given and the approximated matrix

$$\tilde{S} = U^T V_2^N W\Sigma^{-1} = U^T AU \tag{16}$$

can be calculated by projecting A on to U. The eigenvalues λ_i and eigenvectors y_i of $\tilde{S}$ can be calculated with the eigenvalue decomposition, such that $\tilde{S}y_i = \lambda_i y_i$. The dynamic modes Φ are calculated with the matrix U, containing the POD basis of the snapshot matrix V_1^{N-1} and the eigenvectors y as follows:

$$\Phi_i = Uy_i \tag{17}$$

The SVD is used to calculate $U\Sigma W^T$ in Eq. 14 and the eigenvalues and eigenvectors are calculated numerically with the *eig* function in MATLAB. The other calculations are matrix multiplication and inversions, which do not require additional functions. Every dynamic mode represents the dynamic at a specific frequency. The angular frequency of a specific mode can be obtained with

$$\omega_i = \log(\lambda_i)/\Delta t, \tag{18}$$

which can be calculated into the frequency with

$$f_i = \omega_i/2\pi. \tag{19}$$

The frequency resolution of DMD can be calculated analogue to FFT frequency resolution with

$$\Delta f = fps/N_{images} \tag{20}$$

For Condition 1 and Condition 2 with fps = 13180 and N_{images} = 8192 the Δf = 1.61 Hz. For Condition 3 with fps = 22000 and N_{images} = 8192 the Δf = 2.69 Hz.

3.4. Pixel-wise Fast Fourier Transform (FFT) on images

The fft function included in MATLAB is used to calculate the discrete Fourier transform (DFT) of the temporal image sequence matrix for each pixel using a fast Fourier transform algorithm, (Frigo and Johnson, 2005). To reconstruct an image of a mode the spatial magnitude distribution of the specified frequency is plotted. To obtain pressure level distribution, this image is scaled with the reference measurement from a microphone. The frequency resolution of pixel-wise FFT is analogue to DMD resolution for Condition 1 and 2 Δf = 1.61 Hz and Condition 3 Δf = 2.69 Hz.

3.5. Phase averaging

Phase Averaging is commonly used to analyse periodic and quasi periodic phenomena. In this study the phase averaging is performed in the later described condition 1 and 2 measurements, where the camera frame rate is synchronised with the sinusoidal speaker signal. During these measurements 10 images are acquired for each speaker signal period and images corresponding to each phase are averaged.

4. Measurement and Results

4.1. Pressure, Temperature and Frequency calibration of iPSP

Several aluminium samples, coated with iPSP, are prepared and their response to periodic pressure change and pressure and temperature sensitivity is evaluated. The pressure and temperature sensitivity are evaluated in a calibration facility at DLR in Göttingen featuring a pressure sensitivity of 77.0 %/100 kPa and temperature sensitivity of 2.3%/K at reference condition of 100 kPa and 293 K.
The frequency response calibration is performed at the Tohoku University in Japan using an acoustic resonance tube, Sugimoto et al. (2016). The resulting response is shown in the Bode plot in Fig. 6. In order to approximate the gain change due to changing temperature, the iPSP response is modelled using a first order system as proposed by Sugimoto et al. (2016), with an initial time constant $\tau(tau)$ = 25 µs as shown in Fig. 6a. From

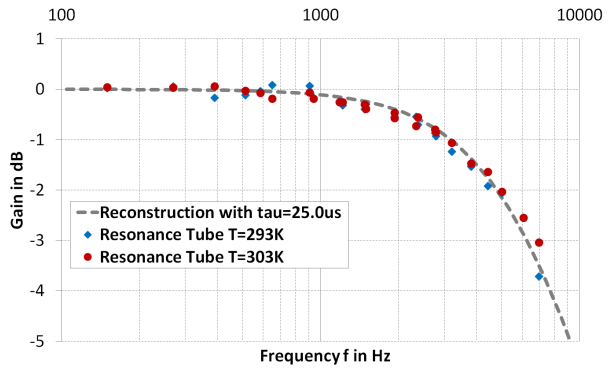

(a) Bode Plot Gain

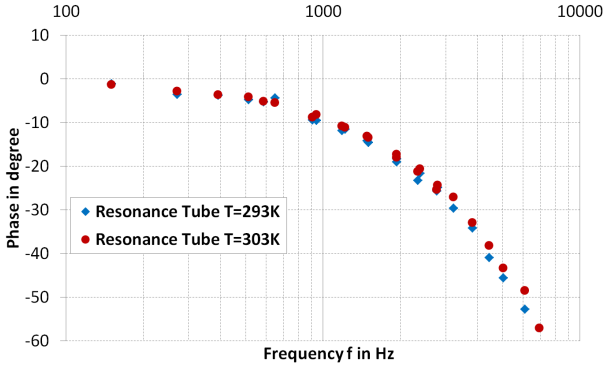

(b) Bode Plot Phase

Figure 6: Frequency calibration

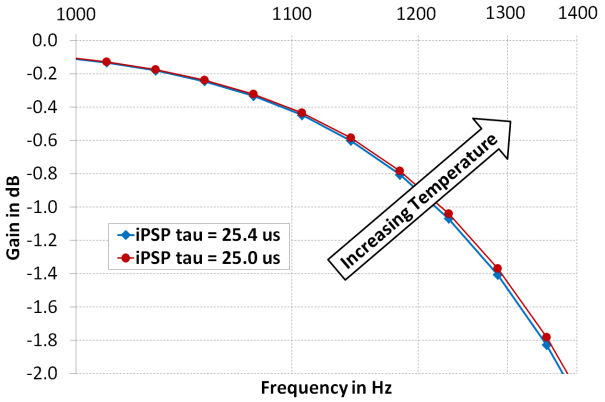

Figure 7: Modelled gain change due to temperature increase of 10 K

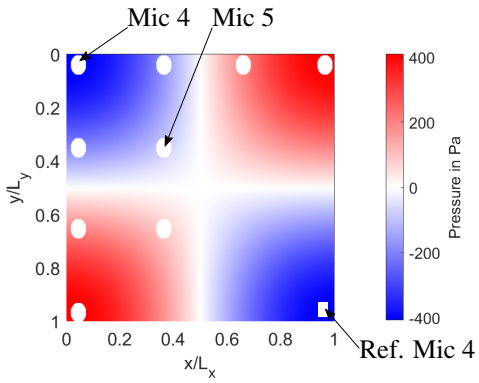

Figure 8: Analytic solution of mode (1 1 0)

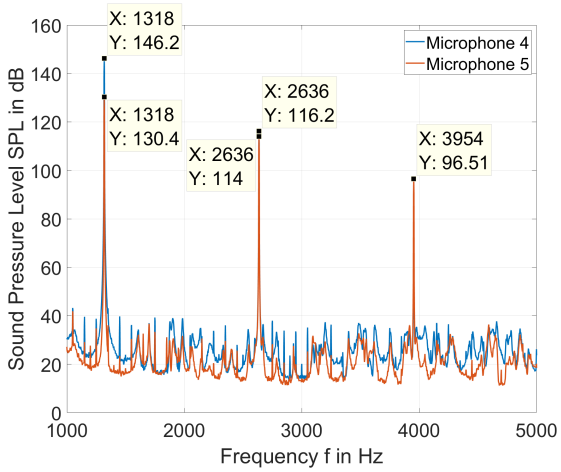

Figure 9: PSD of microphone 4 and 5 in measurement 1

measurements conducted by Sugimoto et al. (2016) with a very similar polymer/ceramic iPSP a decrease of time constant of $\Delta\tau = 0.4$ µs due to increase of Temperature by 10 K is used to model the gain change as shown in Fig. 7. Since the temperature change inside the test section is significantly smaller than $\Delta T < 1$ K the influence of temperature is considered to be negligible.

4.2. Condition 1, Mode (1 1 0), high amplitude

During the measurement of condition 1, the mode (1 1 0) with a frequency of 1318 Hz is excited with a high sound pressure level. The camera is synchronised with the speaker and is capturing images with a frame rate of 13180 Hz. The exposure time of the camera is 64 µs. The 768x768 pixel images are cropped to only show the area of the back wall surface. To reduce the needed memory size and time for further calculations, the image is 2x2 spatial binned. This leads to a final resolution of 278 pixel in y and 358 pixel in x direction. Since the back wall is 168 mm in height and 216 mm in width, the pixel resolution in both direction is 1.65 pixel/mm.
The analytic solution of mode (1 1 0) is shown in Fig. 8. The PSD is calculated for each microphone and the data of microphone 4 and 5 are shown in Fig. 9. Microphone 5 is placed closer to the center of the back wall and is therefore measuring smaller pressure fluctuations. This is also predicted by the analytic solution and therefore confirms the measurement. The PSD is showing that the multiple modes of mode (1 1 0) are excited as well. The mode (2 2 0) with a frequency of 2636 Hz is achieving a SPL of 116.2 dB at microphone 4 and 114 dB at microphone 5. The mode (3 3 0) with a frequency of 3954 Hz is excited with a SPL of 96.5 dB for both microphones.

The analytic solution as presented in Fig. 8 is calculated with pressure levels between 0 and 1 and is then scaled to fit the estimated pressure of the PSD at 1318 Hz.

The scaling is done by calculating the ratio of the resulting values of the mode at the pressure reference region and the particular microphone pressure. So the pressure distribution is calculated with

$$P = \frac{p_{mic}}{I_{ref}} I, \tag{21}$$

where P is the quantitative pressure distribution of the mode, I is the qualitative pressure distribution, p_{mic} is the pressure of the specific microphone and I_{ref} is the pressure reference region of this microphone. To increase the precision of the recalculation, the value of the pressure reference region is taken of an averaged 5 pixel square area. The same scaling procedure is done for the averaged, POD, FFT and DMD mode.
In Fig. 10, the results of the different data reduction methods are shown. All four of the used data reduction methods are able to visualise the mode (1 1 0) in a good agreement to the analytic solution. The pressure field looks similar for each method. The phase averaging method has the advantage over the other three methods, that no additional pressure information is required to quantify the pressure field. But to achieve a better comparison, the averaged result, shown in Fig. 10a, is scaled, with the pressure level from PSD of microphone 4.
To compare the noise reduction efficiency of the different methods, the standard deviations of the pressure from iPSP is calculated at the 5x5 pixel reference position of microphone 4.

The resulting standard deviation (STD) and the signal-to-noise ratio (SNR) are listed in Tab. 1. In the presented test case, FFT appears to have the highest SNR closely followed by DMD. At pressures below the detection limit of the setup, the

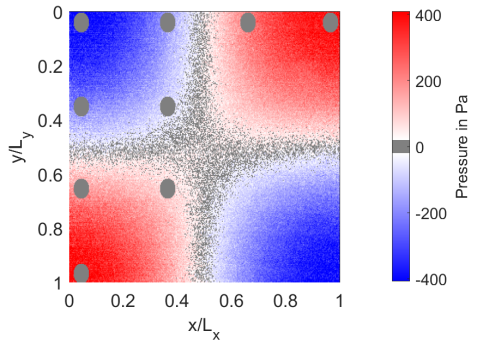

(a) Averaged, calibrated in situ

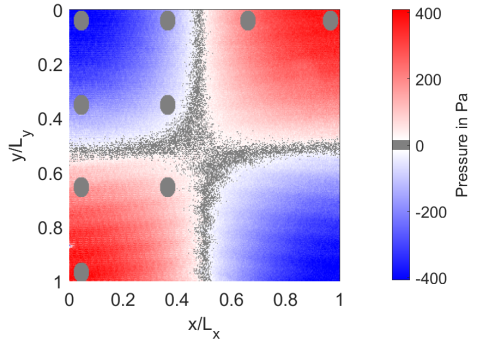

(b) POD

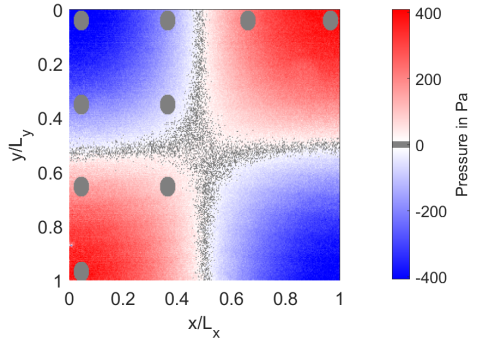

(c) FFT

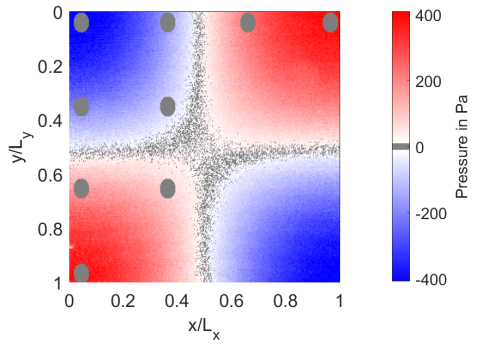

(d) DMD

Figure 10: Results of different data reduction methods, Mode (1 1 0)

Methode	average	POD	FFT	DMD
STD	45.3 Pa	32.8 Pa	23.6 Pa	27.9 Pa
SNR	9.03	11.58	17.35	14.70

Table 1: STD and SNR of different data analysis methods during condition 1, calculated of 5x5 pixel area at position of reference microphone 4

colormap is set to be grey. Sec. 4.3 explains how the pressure detection limit is obtained.
The camera noise pattern is indicated by horizontal lines in the corners of each result image. The FFT and DMD methods are suppressing these patterns more efficiently compared to the POD method. In the averaged result of Condition 1, the camera noise pattern is partially concealed by random noise resulting to the lowest SNR of all four methods.

The specific mode of the camera noise pattern is shown in Fig. 11 with a mode frequency of 608 Hz. The better

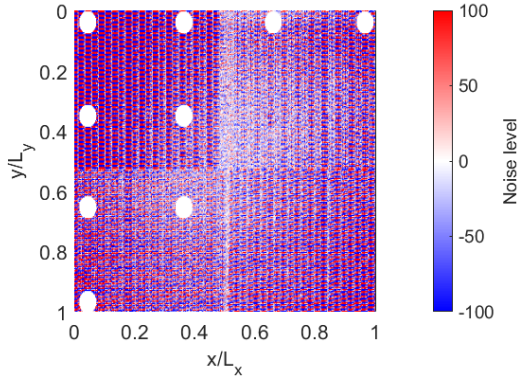

Figure 11: Dynamic mode of the camera noise at 608 Hz

results of the FFT and DMD method relate to their property, to include only patterns which occur at the specific frequency of the investigated mode. The POD and averaged result images contain phenomena of different frequencies and therefore, also the camera noise occurring at 608 Hz.

The averaged images, the FFT, and DMD are further compared by cutting through the resulting images and plotting one line for each method. To enhance the SNR of the lines and improve the comparison, 5 parallel pixels along the center line, which roughly compare to the diameter of the microphone, are averaged. Furthermore, a smoothing spline curve is fitted through the pressure points of the averaged center line. For some points on the line the standard deviation of the 5 parallel pixel is calculated and shown with error bars. In Fig.12 the cuts in x direction at $y = 8$ mm or $y/L_y = 0.05$, and $y = 108$ mm or $y/L_y = 0.64$ are shown. Since the lines average several pixels in y direction, they contain information from $y = 6.5$ mm to 9.5 mm and $y = 106.5$ mm to 109.5 mm. The plot confirms that the FFT and the dynamic mode features a higher SNR than the average method. Furthermore, it can be seen that each method is following the analytic solution. This is the case for the line

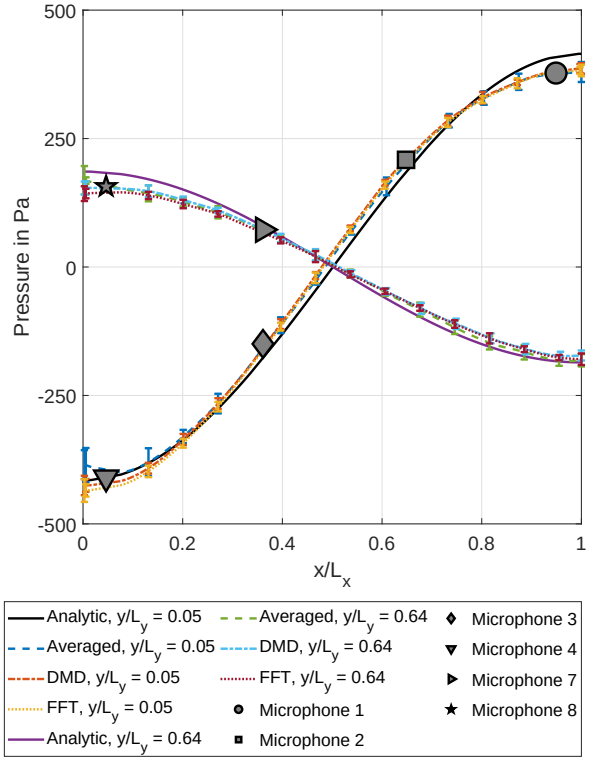

Figure 12: Cut through the different results of mode (1 1 0)

at $y/L_y = 0.05$, where the microphone 1, 2, 3, and 4 are positioned. The SPLs of microphone 1 - 8 at 1318 Hz are also integrated in Fig. 12. It is notable, that all microphones have similar pressures as the scaled pressure of the resulting modes at the position of the microphones. Also the line at $y/L_y = 0.64$ is in a good agreement with the analytic solution and with the pressure references from related microphones. For example, the pressure of the PSD calculation of microphone 7 at 1318 Hz is 72 Pa. The estimated pressure from the analytic solution, the average image, the FFT, and the DMD is between 68 and 75 Pa. Therefore, the pressure scaling for the whole mode using one reference microphone is usable. Figure 12 is also indicating, that the iPSP is able to detect lower pressure levels. Between the microphone 7, with 72 Pa, and the center of the back wall, with very low pressure levels, the paint is still detecting pressure information. The gained pressure in this region is also similar to the analytic solution.

The investigation of condition 1 reveals, that measurements of acoustic applications with iPSP developed by the DLR Göttingen are possible. The used iPSP setup is able to detect acoustic pressure fluctuations of good coherence with the analytic solution and the microphone pressures. From the different data analysis methods, FFT and DMD are the most powerful and are delivering results with the best SNR. But to obtain quantitative pressure level information, a pressure reference device, such as a microphone, is needed.

4.3. Condition 2, Mode (1 1 0), low amplitude

During the measurement of condition 2 the mode (1 1 0) is excited with low speaker output. This is done to investigate the limit of the lowest detectable pressure level. The excitation frequency is the same as in condition 1 at 1318 Hz. Also the settings of the camera are the same, with a frame rate of 13180 Hz and an exposure time of 64 µs. The SPL of microphone 4 and microphone 5 are 129.2 dB (57.68 Pa) and 112.9 dB (8.83 Pa), respectively.

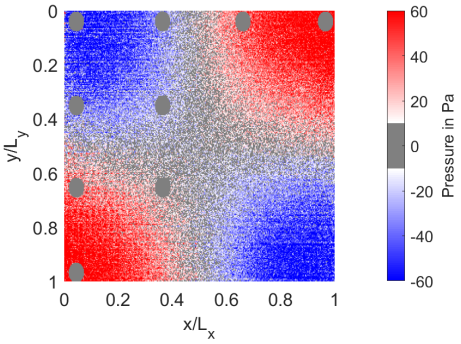

(a) Phase averaged, calibrated in situ

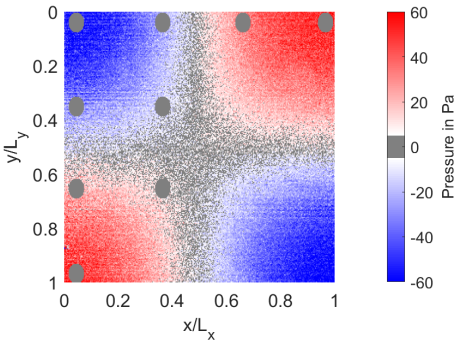

(b) FFT

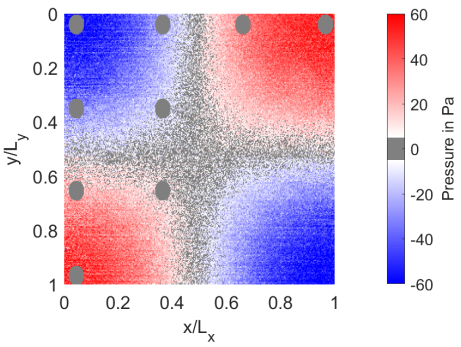

(c) DMD

Figure 13: Results of different data reduction methods, Mode (1 1 0)

To increase the SNR, the measurement is performed 8 times. The phase averaged image, the FFT and the dynamic modes are calculated for each measurement separately. The 8 phase averaged results are organised to the same phase and averaged to

one. The same procedure is done for the FFT and the dynamic modes, first the result of a single measurement is calculated with the specific data analysis method and later the results are averaged. Therefore, each pressure distribution contains information from 65536 images.
The resulting pressure distributions are shown in Fig. 13. The pressure of the modes is scaled as described in condition 1 with the pressure level of microphone 4 and its reference region with Eq. 21.

Methode	average	FFT	DMD
STD	22.8 Pa	10.1 Pa	11.6 Pa
SNR	2.54	5.76	5.00

Table 2: STD and SNR of different data analysis methods for condition 2, calculated on a 5x5 pixel area at the reference position of microphone 4

The resulting STD and the SNR of the data analysis methods at the 5x5 pixel reference area of microphone 4 are shown in Tab. 2. The comparison shows that the noise reduction is more efficient by using the FFT or DMD method over the phase average method. However, all data analysis methods are capable of detecting the pressure field, which is distributed similar to the results in condition 1. The phase averaged pressure field is noisier than the other two results and is detecting slightly different pressure magnitudes for positive and negative pressure. This is seen in the corner of the acoustic box at positive pressure. At these areas, the pressure is above 80 Pa, which is neither detected by the microphones nor by the FFT or DMD method.
To obtain the pressure level limit with the used setup at a frequency of 1318 Hz, only the magnitude of the mode is plotted. The mode is cut again, with a similar procedure to Condition 1, at $y/L_y = 0.05$ and $y/L_y = 0.64$ in x direction and shown in Fig. 14. In this Figure, the x axis is cropped to show the x direction between 45 and 170 mm or $x/L_x = 0.21$ and $x/L_x = 0.79$. The pressures levels of the microphones 2, 3, and 7 at the mode frequency are included as well. The pressure levels of the FFT and the dynamic mode are in a good agreement with the pressure levels of the microphones. The smallest pressure level of 114 dB (10 Pa) is measured by microphone 7. Figure 14 reveals, that even smaller pressure levels can be detected by this iPSP setup. The analytic solution predicts a pressure level reduction to 0 Pa in the center of the back wall. However, by looking at the magnitude of both methods the obtained pressures do not follow the analytic solution below 5 Pa. No pressure information is gained and only noise occurs around the center of the back wall, where the pressure levels are below 5 Pa. Therefore, the pressure detection limit with this setup at a frequency of 1318 Hz is at 5 Pa.
The DMD is a very powerful tool to separate the mode of interest from other acoustic modes or modes containing noise. In a low pressure level application, the pressure recalculation using a reference pressure is working with the DMD method better than with the phase averaging method. However, the data required to obtain results for this low pressure case is high. A hard disc storage of 75 Gigabyte and about 64 gigabyte RAM

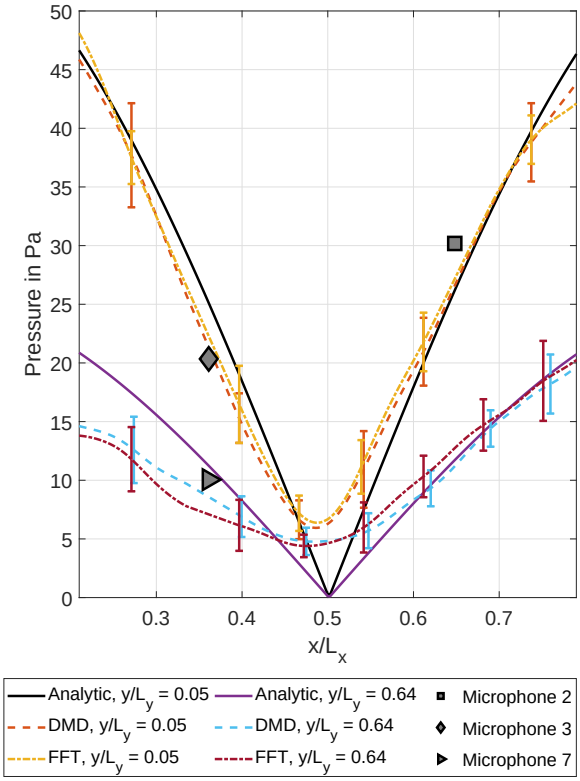

Figure 14: Cut through the magnitude of low amplitude mode (1 1 0)

are required to calculate the dynamic modes from 8192 images. Also, the FFT method is capable of detecting the pressure field with similar precision but with less resources. The calculation from 8192 images needed 16 gigabyte RAM. Image binning or spatial image division into smaller regions can also be used to reduce resource requirements.

4.4. Condition 3, white noise excitation

Condition 3 is set up to test the iPSP for acoustic phenomena with multiple mode appearances. The speakers are driven with a white noise signal. The camera is running independently at a frame rate of 22000 Hz with an exposure time of 36 µs. Due to the dimension of the acoustic box and the white noise excitation, several modes are induced, each with a specific frequency and power. Therefore, the PSD is more similar to a broadband phenomena than a single frequency phenomena as in condition 1 and 2. In Fig. 15, the PSD for the multi-mode excitation is shown and reveals a variety of modes with different SPLs. Microphone 1 measures peaks with SPLs between 110 dB (6.32 Pa) and 132.5 dB (84.34 Pa). Each peak represents a specific mode or mode combination. For example, the mode at a frequency of 2217 Hz with a SPL of 130.7 dB (68.55 Pa) has the mode number (1 2 0). Hence, half of a wave is fitted between the walls in x direction and one period is fitted between the walls in y direction. This mode is a superposition of the mode (1 0 0) and (0 2 0). The modes at frequencies of 2532

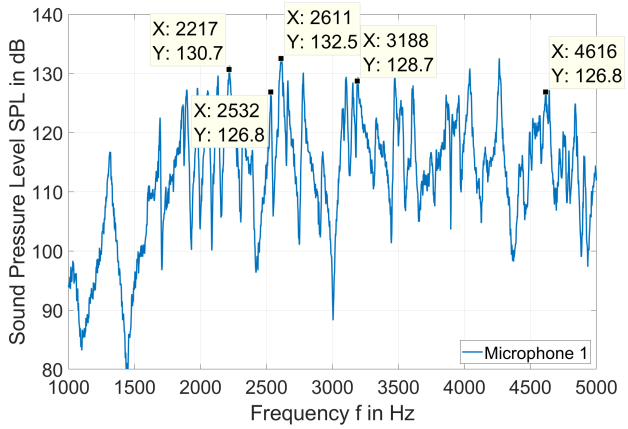

Figure 15: Power spectral density of microphone 1 in measurement 3

Hz and 4615 Hz have the mode number (2 1 1) and (3 2 2), respectively. The three modes are investigated by calculating the DMD of the images captured in condition 3 and extracting the dynamic modes for the given frequencies. The resulting pressure distributions are shown in Fig. 16.

According to the PSD of the microphone 1, the mode (1 2 0) has one of the highest pressure levels in the condition 3 measurement. The SPL measured by microphone 1 for this mode is 130.7 dB (68.55 Pa) at a frequency of 2217 Hz. The extracted dynamic mode is shown in Fig. 16a.
The next detected mode is the mode (2 1 1) with an excitation frequency of 2532 Hz. This mode is induced with a lower amplitude, microphone 1 is measuring a SPL of 126.8 dB (43.8 Pa). Compared to the other extracted dynamic modes in this evaluation, this mode is distorted more by the camera readout noise patterns. This pattern can be seen in the whole image and not only in the corners. These pattern are also occurring in dynamic modes with frequencies around 2532 Hz. They also feature higher noise levels and lower SNR. Because of the pronounced camera noise this mode shows a higher pressure level detection limit of 8 Pa (112 dB) at a frequency of 2532 Hz.
The dynamic mode (3 2 2) has a frequency of 4615 Hz. The pressure field on the back wall is a superposition of the modes (3 0 0) and (0 2 0). The wave in z-direction has no influence on the pressure distribution of the back wall. The pressure distribution of the extracted dynamic mode is shown in Fig. 16c. Although the pressure levels are very similar compared to the pressure levels in mode (2 1 1), the SNR is slightly increased. This could be a function of to the camera read out noise which is slightly less pronounced at a frequency of 4615 Hz compared to the modes with frequencies around 2532 Hz. The iPSP setup is detecting in mode (3 2 2) pressure levels above 7 Pa (110.9 dB), which is 1 Pa lower than the detection limit of mode (2 1 1). The selected DMD modes show that, with the current setup, it is possible to extract pressure distributions of modes with frequencies up to 5000 Hz.
During the white noise excitation the acoustic box accommodates several modes within a close frequency range. In example, the modes (2 2 0) and (3 1 0) with theoretical excitation frequencies of 2607 Hz and 2614 Hz, respectively. The PSD, which has a frequency resolution of 3.7 Hz, shows at this frequency range only one peak. It can be assumed, that the mode (2 2 0) and (3 1 0) overlap with each other with an indicated frequency peak at 2611 Hz.
The weighting w for the overlapping modes can be determined by a reconstruction of the modes using calibrated microphone data. To obtain the weighting factors the microphone data, which is acquired with a sampling frequency of 240 kHz for 20 seconds, are processed using an overlap of 50% and a fast Fourier transform block size of 2^{16} samples, with a Hann window, yielding 144 averages and a narrow band frequency resolution of 3.7 Hz. To determine the amplitudes and phase re-

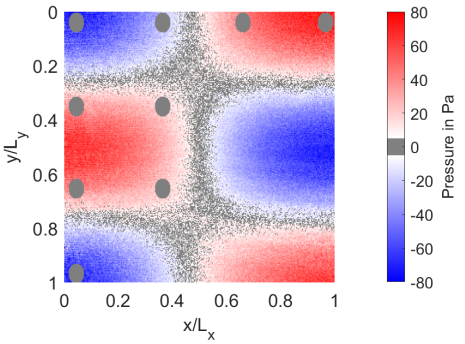

(a) Mode (1 2 0) at 2217 Hz

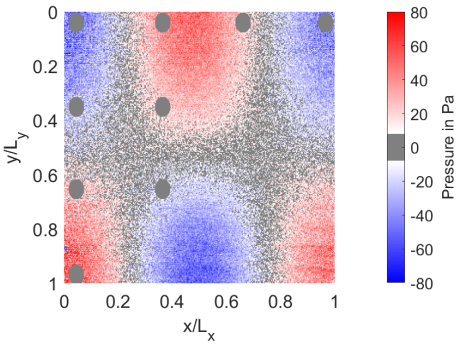

(b) Mode (2 1 1) at 2532 Hz

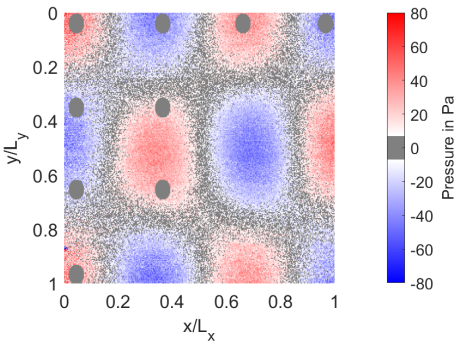

(c) Mode (3 2 2) at 4615 Hz

Figure 16: Selected DMD modes at specific frequencies

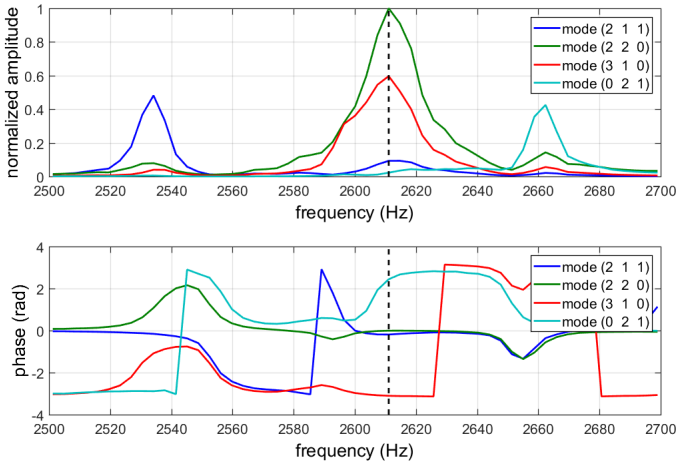

Figure 17: Solution of linear equations using microphones 1-9)

lations of the individual modes, a system of equations based on equation 4 is established. With 9 microphone signals this yields 9 equations for a large number of possible modes. In order to reduce the number of unknowns the relevant modes in the vicinity of 2611 Hz are determined with equation 3 in the range of 2.5 kHz to 2.7 kHz including 4 modes: (2 1 1), (2 2 0), (3 1 0) and (0 2 1) and thus an over-determined system of equations with 4 unknowns. Figure 17 depicts the solution of this system of equations in terms of amplitude and phase. It shows that at the 2611 Hz the modes (2 2 0) and (3 1 0) are the most dominant, with normalised amplitudes of $w = 1$ for the mode (2 2 0) and $w = 0.6$ for the mode (3 1 0). For these modes the phase difference at 2611 kHz is approximately π. The normalised amplitudes can be used as weighting factors for the analytic solution. The analytic solution of the overlapping modes is then calculated by a sum of the 2 modes multiplied by the weighting factor w. Figure 18 shows the analytic solution in comparison to the DMD and FFT results obtained from the iPSP measurement.

The comparison shows a very good agreement.

5. Conclusion

In a typical application, the Aeroacoustic Wind Tunnel in Hannover provides sound pressure levels up to 136 dB (126 Pa) with frequencies between 1000 Hz and 4000 Hz.

The minimal detectable pressure level limit which is necessary for the usage of fast response Pressure-Sensitive Paint inside the AWT is assumed to be around 134 dB (100 Pa). The results of the experimental evaluations show that the iPSP developed at DLR is capable of detecting acoustic pressure levels in this range and below. Advanced data reduction methods such as POD and DMD are used and compared to analytic solutions, microphone measurements and conventional phase average and FFT analysis of the iPSP data. The condition 1 measurement reveals, that time step images detected with iPSP are not usable without further post processing, due to a low SNR in each image. However, the data analysis methods

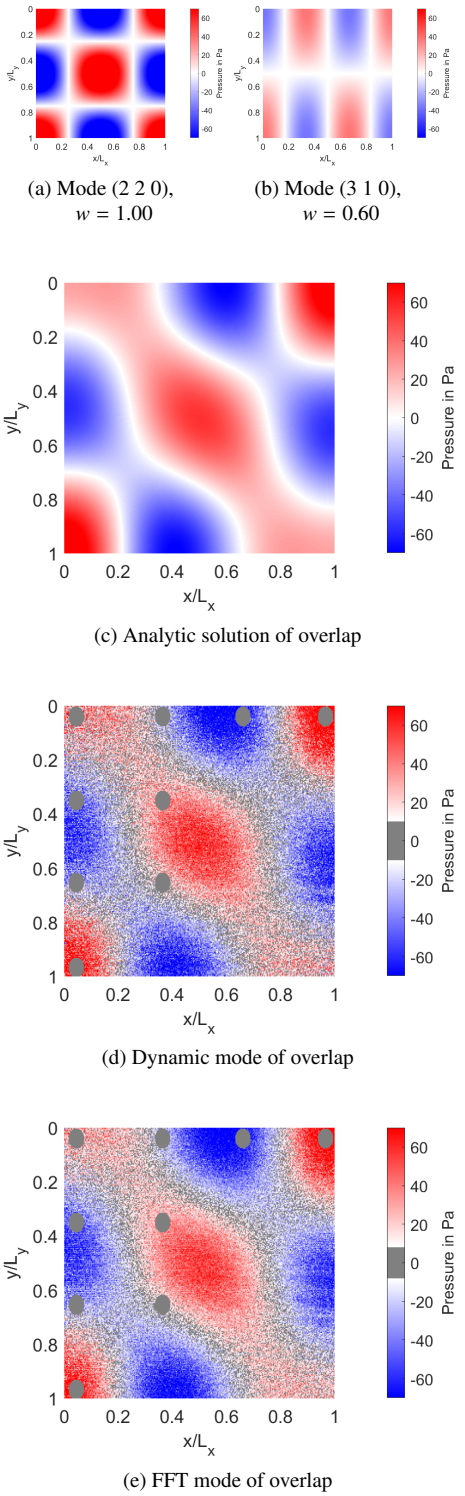

(a) Mode (2 2 0), $w = 1.00$

(b) Mode (3 1 0), $w = 0.60$

(c) Analytic solution of overlap

(d) Dynamic mode of overlap

(e) FFT mode of overlap

Figure 18: Pressure distribution of overlapping modes at a frequency of 2611 Hz

phase averaging, proper orthogonal decomposition, fast Fourier transform, and dynamic mode decomposition are capable of increasing the SNR significantly.

The phase averaging method is simple to use and to implement

which also allows for a direct pressure calculation using the Stern-Volmer equation. This calculation does not need a reference pressure device on the surface investigated with iPSP. This makes an implementation of the iPSP possible on surfaces without pressure reference devices e.g. on turbine blades inside the AWT. However, the calculation of small pressure levels in acoustic applications is difficult and a temperature correction is often required to remove any local or global offsets which would usually lead to pressure level distortions. Additional measurement of the surface temperature needs to be performed simultaneously and could significantly complicate the setup for the phase averaging method. Furthermore, multi-frequency phenomena can not be investigated with the averaging method, except in cases where the frequency of those phenomena are known or measured directly. Therefore, concluding from the results of this evaluation, especially in condition 2, the phase averaging method is only recommended for pressure levels above 50 Pa (128 dB) and with single frequency phenomena.
POD, closely related to SVD, is only considered in condition 1 measurement. The extracted POD mode shows a similar SNR as the extracted dynamic mode, but with a significantly pronounced camera read out noise pattern. Especially in multi-frequency measurements, the determination of specific mode frequencies is required, in which case DMD or FFT are the preferable methods.
Within the acoustic box setup, the more common FFT analysis delivers comparable results to DMD. Since the calculation time of FFT is one order of magnitude lower than for DMD, it should also be considered for post processing.
The used setup, together with the DMD or FFT data reduction, is capable of detecting pressure levels as low as 5 Pa (108 dB). The detectable pressure level limit of the setup is varying with the frequency, which can be related to the camera noise being more pronounced at certain frequency bands. The detectable pressure level limits in this measurement are 5 Pa (108 dB) at 1318 Hz, 8 Pa (112 dB) at 2538 Hz, and 7 Pa (111 dB) at 4615 Hz.

The white noise excitation proved the capability of the iPSP to detect multiple frequency phenomena, even with pressure levels below 20 Pa (120 dB). Furthermore, DMD and FFT are capable of extracting modes of interest with specific frequency and increase the SNR significantly. The drawback of the DMD and FFT methods is that a pressure reference device (e.g. microphone) is needed to calculate the correct pressure levels. This device must have a fast response time and should be able to detect low pressure amplitudes. The same device can also be used to calculate and reconstruct mode structures analytically.

Overall, the iPSP together with DMD and FFT is capable of measuring acoustic pressure phenomena, similar to the acoustic phenomena found inside the AWT. Pressure levels above 20 Pa (120 dB) are well observed and the minimal detectable pressure level limit of 5 Pa at 1318 Hz is a good basis for future development and measurements.

6. Acknowledgement

The authors would like to thank and acknowledge Akif Mumcu, M.Sc., Dipl.-Ing. Michael Henke and Prof. Jörg Seume from Leibniz University Hannover, Institute of Turbomachinery and Fluid Dynamics for their valuable support. Furthermore we would like to thank Dr. Yorita Daisuke, Dr. Christian Klein, Dr. Daniel Ernst, Dr. Carsten Spehr, Carsten Fuchs and Tobias Kleindienst from German Aerospace Center (DLR), Institute of Aerodynamics and Flow Technology, Göttingen for their important support. Also many thanks to Miku Kasai and Prof. Keisuke Asai from Tohoku University for allowing and performing the unsteady PSP calibrations.

7. References

Ali, M.Y., Pandey, A., Gregory, J.W., 2016. Dynamic mode decomposition of fast pressure sensitive paint data. Sensors (Basel, Switzerland) 16. doi:10.3390/s16060862.

Bartelt, M., Laguna, J.D., Seume, J.R., 2013. Synthetic sound source generation for acoustical measurements in turbomachines, in: Volume 6C: Turbomachinery, ASME. p. V06CT39A005. doi:10.1115/GT2013-95045.

Disotell, K.J., Gregory, J.W., 2011. Measurement of transient acoustic fields using a single-shot pressure-sensitive paint system. The Review of scientific instruments 82, 075112. doi:10.1063/1.3609866.

Frigo, M., Johnson, S.G., 2005. The design and implementation of FFTW3. Proceedings of the IEEE 93, 216–231. Special issue on Program Generation, Optimization, and Platform Adaptation.

Gregory, J., 2004. Porous pressure-sensitive paint for measurement of unsteady pressures in turbomachinery. 42nd AIAA Aerospace Sciences Meeting and Exhibit doi:10.2514/6.2004-294.

Gregory, J.W., Sakaue, H., Liu, T., Sullivan, J.P., 2014. Fast pressure-sensitive paint for flow and acoustic diagnostics. Annual Review of Fluid Mechanics 46, 303–330. doi:10.1146/annurev-fluid-010313-141304.

Gregory, J.W., Sullivan, J.P., Wanis, S.S., Komerath, N.M., 2006. Pressure-sensitive paint as a distributed optical microphone array. The Journal of the Acoustical Society of America 119, 251–261. doi:10.1121/1.2140935.

Liu, T., Sullivan, J.P., 2005. Pressure and Temperature Sensitive Paints. Experimental Fluid Mechanics, Springer-Verlag Berlin Heidelberg, Berlin, Heidelberg. doi:10.1007/b137841.

McGraw, C.M., Shroff, H., Khalil, G., Callis, J.B., 2003. The phosphorescence microphone: A device for testing oxygen sensors and films. Review of Scientific Instruments 74, 5260–5266. doi:10.1063/1.1626009.

Möser, M., 2012. Elektroakustische wandler für luftschall, in: Möser, M. (Ed.), Technische Akustik. Springer Berlin Heidelberg, Berlin, Heidelberg, pp. 355–390. doi:10.1007/978-3-642-30933-5_11.

Noda, T., Nakakita, K., Wakahara, M., Kameda, M., 2018. Detection of small-amplitude periodic surface pressure fluctuation by pressure-sensitive paint measurements using frequency-domain methods. Experiments in Fluids 59, 94. URL: https://doi.org/10.1007/s00348-018-2550-z, doi:10.1007/s00348-018-2550-z.

Pastuhoff, M., Yorita, D., Asai, K., Alfredsson, P.H., 2013. Enhancing the signal-to-noise ratio of pressure sensitive paint data by singular value decomposition. Measurement Science and Technology 24, 075301. doi:10.1088/0957-0233/24/7/075301.

Peng, D., Wang, S., Liu, Y., 2016. Fast psp measurements of wall-pressure fluctuation in low-speed flows: improvements using proper orthogonal decomposition. Experiments in Fluids 57, 45. URL: https://doi.org/10.1007/s00348-016-2130-z, doi:10.1007/s00348-016-2130-z.

Pierce, A.D., 1981. Acoustics: an introduction to its physical principles and applications. McGraw-Hill New York.

Ruhe, A., 1984. Rational krylov sequence methods for eigenvalue computation. Linear Algebra and its Applications 58, 391–405. doi:10.1016/0024-3795(84)90221-0.

Schmid, P.J., 2010. Dynamic mode decomposition of numerical and experimental data. Journal of Fluid Mechanics 656, 5–28. doi:10.1017/S0022112010001217.

Stoica, P., Moses, R.L., 2005. Spectral analysis of signals. Pearson Prentice Hall, Upper Saddle River, NJ.

Strang, G., 2003. Lineare Algebra. Springer Berlin Heidelberg, Berlin, Heidelberg. doi:10.1007/978-3-642-55631-9.

Sugimoto, T., Sugioka, Y., Numata, D., Nagai, H., Asai, K., 2016. Characterization of frequency response of pressure-sensitive paints. AIAA Journal 55, 1460–1464. URL: https://doi.org/10.2514/1.J054985, doi:10.2514/1.J054985.

Welch, P., 1967. The use of fast fourier transform for the estimation of power spectra: A method based on time averaging over short, modified periodograms. IEEE Transactions on Audio and Electroacoustics 15, 70–73. doi:10.1109/TAU.1967.1161901.